A Model of the Closed Form of the Nicotinic Acetylcholine Receptor M2 Channel Pore

Sanguk Kim, Aaron K. Chamberlain, and James U. Bowie
Department of Chemistry and Biochemistry and UCLA-Department of Energy Center for Genomics and Proteomics, University of California, Los Angeles, Los Angeles, California

ABSTRACT The nicotinic acetylcholine receptor is a neurotransmitter-gated ion channel in the postsynaptic membrane. It is composed of five homologous subunits, each of which contributes one transmembrane helix—the M2 helix—to create the channel pore. The M2 helix from the δ subunit is capable of forming a channel by itself. Although a model of the receptor was recently proposed based on a low-resolution, cryo-electron microscopy density map, we found that the model does not explain much of the other available experimental data. Here we propose a new model of the M2 channel derived solely from helix packing and symmetry constraints. This model agrees well with experimental results from solid-state NMR, chemical reactivity, and mutagenesis experiments. The model depicts the channel pore, the channel gate, and the residues responsible for cation specificity.

INTRODUCTION

Nicotinic acetylcholine receptors (AChR) are neurotransmitter-gated ion channels that control electrical signaling between nerve and muscle cells. These receptors have received considerable attention because of their physiological importance. In the neuromuscular junction, AChRs detect the neurotransmitter, acetylcholine, and propagate the nerve impulse by opening and allowing an influx of extracellular sodium ions. Nicotine and the snake venom, α-bungarotoxin, also bind these receptors with agonistic and antagonistic effects, respectively. In addition, 85% of patients with the autoimmune disease, myasthemia gravis, have elevated levels of AChR antibodies in their blood (Patrick and Lindstrom, 1973; Vincent et al., 2003).

The best-studied AChR consists of five subunits (α, α, β, γ, and δ) and opens upon binding of acetylcholine (Ach) near the subunit interfaces of the two α-subunits (Corringer et al., 2000; Karlin, 2002). Each subunit contains four α-helical membrane-spanning segments, labeled M1–M4. The M2 segments form the pore, the cation selectivity filter, and the gate of the closed AChR channels (Hucho et al., 1986; Imoto et al., 1986; Lester, 1992; White and Cohen, 1992; Unwin, 1993, 1995). Chemical modification data suggest the amino-terminal part of M1 segments may also contribute to the channel lining (Akabas and Karlin, 1995; Zhang and Karlin, 1997). Isolated peptides of the M2 transmembrane (TM) helix self assemble in lipid bilayers, and can form cation-selective ion channels, however, suggesting that the M1 segments may not be critical for ion permeation (Oiki et al., 1988; Opella et al., 1999).

Recently, an image of the AChR channel came from sophisticated cryo-electron microscopy (EM) experiments on tubular crystals and reveals the basic architecture of the protein at 4 Å resolution (Miyazawa et al., 2003). Based on their low-resolution electron density map, Miyazawa et al. proposed a preliminary model of the membrane domain including the channel (Protein Data Bank (PDB) code 1OED). No refinement was carried out on the model, however, and side-chain details are difficult to see at this resolution. Thus, it is appropriate to validate the model with other available data. We found the cryo-EM model is incompatible with the solid-state NMR data on M2 peptides (Opella et al., 1999), and appears to be inconsistent with some of the chemical modification experiments conducted on the full-length protein (Leonard et al., 1988; Pascual and Karlin, 1998).

We built a structure of the M2 channel-lining segments using a method we have developed for modeling transmembrane helical bundles. The M2 segments in our model differ substantially from those of the cryo-EM model in helical tilt, the identity of the pore-lining residues and the helix-helix packing interactions. Our model shows excellent agreement with the solid-state NMR data and is consistent with much of the other experimental data (Leonard et al., 1988; Revah et al., 1991; Pascual and Karlin, 1998; Opella et al., 1999). The atomic detail of our M2 channel model identifies residues that are pore lining, external, and helix-helix packing. Our model also provides possible explanations for the channel gate and for the cation specificity of the pore.

METHODS

Generation of the channel model

We built an AChR M2 channel model using our algorithm that was shown to accurately model the structures of TM helix homo-dimers, tetramers, and pentamers (Kim et al., 2003). We first built M2 TM helix monomers from

Submitted December 29, 2003, and accepted for publication April 22, 2004.

Address reprint requests to James Bowie, Dept. of Chemistry and Biochemistry and UCLA-Department of Energy Center for Genomics and Proteomics, Boyer Hall, University of California, Los Angeles, 611 Charles E. Young Dr., E. Los Angeles, CA 90095-1570. E-mail: bowie@mbi.ucla.edu.

0006-3495/04/08/792/08 $2.00

doi: 10.1529/biophysj.103.039396

the *Torpedo marmorata* sequences (Fig. 1 *a*) using the InsightII Biopolymer package (Accelrys, San Diego, CA) and backbone torsion angles of $\phi = -65°$ and $\psi = -40°$ (Smith et al., 1996). The side-chain rotamers were chosen using the backbone-dependent rotamer library program, SCWRL (Bower et al., 1997). To find the best helix orientations, we began with 400 pairs of helices in random positions and optimized their packing with a Monte Carlo (MC) minimization procedure using a softened van der Waals potential. This optimization resulted in 400 well-packed helix pair structures. The internal backbone and side-chain positions were kept fixed during the minimizations, but the relative positions of the helices were given all six degrees of freedom. The simulations were stopped after 100,000 MC steps or if 15,000 steps occurred without moving to a lower energy. All six orientation parameters were changed during a step and the same step was repeated, if the previous step resulted in lower energy. The step size in each parameter was randomly selected. The temperature was initially set at 500 K and decreased linearly to 0.1 K over the first 50,000 steps.

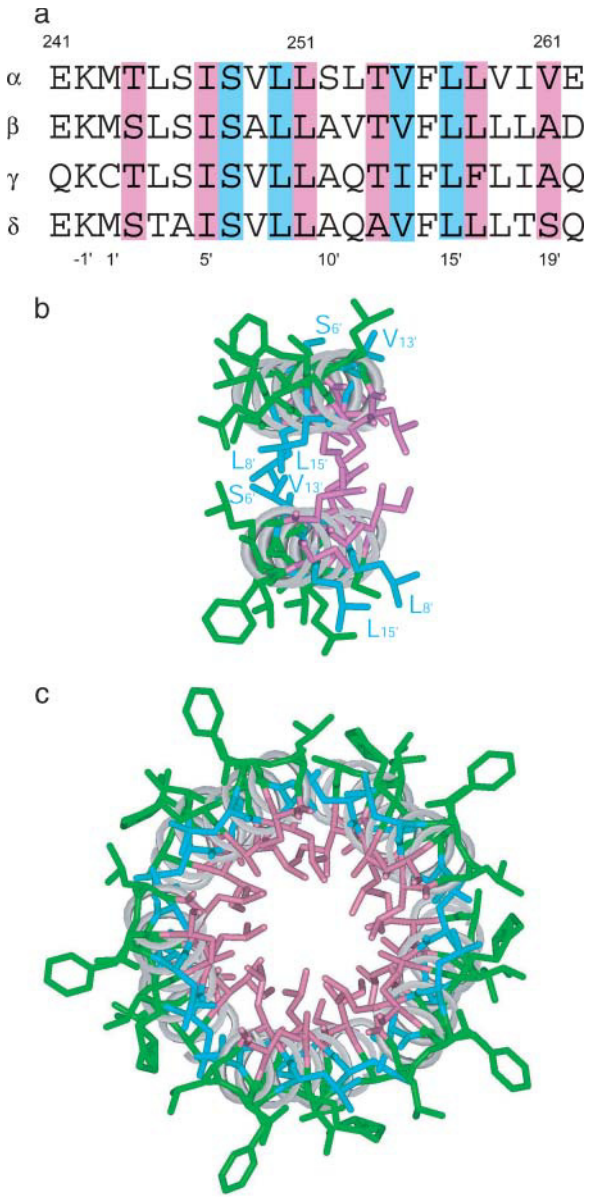

FIGURE 1 Amino acid sequences and the model structure of AChR M2 channel. (*a*) The sequences of M2 segments from *Torpedo marmorta*. The numbers above the sequence are the α-subunit numbering and the corresponding numbers ($-2'$–$20'$) shown at the bottom are used in the manuscript. The pore-lining (*pink*) and helix packing (*blue*) residues of the M2 pentameric channel are indicated. (*b*) The packing between pairs of helices. The external residues are green. (*c*) The AChR M2 model viewed down the fivefold axis from the cytoplasm.

After the MC simulations, the dimer structures were filtered to remove structures incompatible with the pentameric symmetry. That is, we selected only those helix pairs in which the difference in the angles of rotation about the two helical axes was $108° \pm 10°$. We then clustered the remaining structures by Cα RMS distances using NMRCLUSTER (Kelley et al., 1996). The median model from the largest cluster was selected as our final predicted structure. From the 400 MC optimized structures of the δ-subunit, five were consistent with the pentameric symmetry. These structures formed a single cluster and are essentially identical having a Cα RMSD spread of 0.2 Å. Separate simulations with α-subunit M2 helices resulted in an identical structure having a Cα RMSD of only 0.15 Å to the δ-structure. Thus, we found the same structure for both the α- and δ-M2 helices.

To build the pentameric M2 channel structure, we duplicated the structure of the helix pairs by overlaying one helix of the dimer with the other three times. This duplication creates a five-fold rotational symmetry axis, which represents the center of the pore. We calculated the positions of the pore axis by averaging the positions of the equivalent Cα atoms in the five subunits. Optimization of the pentamers was performed in vacuo by the crystallography and NMR system (CNS version 1.1, Brunger et al., 1998). The inter-helical Cα-Cα distances <7.5 Å between the modeled helix pairs were used as restraints for the pentamer structures with additional restraints to maintain the helical backbone. We energy minimized the structures with three rounds of 200 steps using a dielectric constant of 1 and the nonbond cutoff of 13 Å.

2D solid state NMR PISEMA data simulation

PISEMA (polarization inversion spin exchange at the magic angle) experiments demonstrated remarkable sensitivity to the topology of transmembrane peptides through correlated spectra of anisotropic dipolar and chemical shift interactions (Wu et al., 1994; Marassi and Opella, 2000; Wang et al., 2000). 2D solid state NMR PISEMA spectra were simulated from the α-helical coordinates of the M2 models as described (Kim and Cross, 2002). The pore axis of the pentamer channel was assigned to be the axis of the bilayer normal and consequently the axis of the magnetic field. We used the principal values of the ^{15}N chemical shift tensors ($\delta_{33} = 64$ ppm, $\delta_{22} = 77$ ppm, $\delta_{11} = 217$ ppm) from the published solid state NMR data (Ramamoorthy et al., 1995) and a dipolar magnitude value of 10.735 kHz, although it should be noted there are some variations in tensor element magnitudes within a helix (Chekmenev et al., 2004). The values take into account some modest local dynamics of the peptide planes. A typical relative orientation (θ) between the δ_{11} chemical shift tensor element and $\nu_{\|}$ of the dipolar tensor equal to 17° was used (Marassi and Opella, 2000; Wang et al., 2000). The solid state NMR experimental data for the AChR M2 peptide in oriented lipid bilayers is taken from the data of Marassi et al. (1999). To facilitate comparisons, we used ideal helices aligned to the M2 helices in the PDB file 1OED to create the PISA wheel pattern for the cryo-EM model.

RESULTS AND DISCUSSION

The model structure of the M2 channel

The AchR subunits are homologous and the M2 helices show significant sequence identity (Fig. 1 *a*). The numbering used here and that of the α-subunit are also shown. We decided to model the structure of a δ-subunit M2 homopentamer, because the M2 peptide from this subunit

can form a cation selective pore and clearly adopts a defined structure in lipid bilayers (Opella et al., 1999). The sequence similarity of the subunits indicates that the structures formed with different subunit compositions should be essentially identical to the δ-subunit homopentamer.

We modeled the pentameric, AChR M2 segment using our recently developed algorithm that is effective at predicting homo-oligomeric TM helix bundles (Kim et al., 2003). Without aid of experimental data, this method successfully built the TM helix dimer structure of glycophorin A, the tetramer structure of the influenza virus M2 proton channel and the pentamer structure of phospholamban (Kim et al., 2003). We built the AChR M2 δ-pentamer utilizing the following steps: 1), Starting with two δ-subunit helices in random positions, a collection of 400 well-packed helix pairs was generated using an MC minimization. 2), The structures lacking the pentameric symmetry were eliminated. 3), The remaining structures were clustered and a representative of the largest cluster was selected. And 4), the pentameric channel was built by replicating the selected helix pair structure around a pore axis and the pentamer was energy minimized.

Our model of the homo-pentameric M2 δ-subunit channel is shown in Fig. 1. The helices have a helix-crossing angle of $+15°$ (Fig. 1 *b*), which is among the most favorable packing angles between helices in membrane proteins (Bowie, 1997). This positive crossing angle gives the pore a left-handed twist. The pore-lining residues are Ser-2′, Ile-5′, Leu-9′, Ala-12′, and Leu-16′ (*pink*). The helix-helix packing residues are Ser-6′, Leu-8′, Val-13′, and Leu-15′ (*blue*). Ser-6′ and Val-13′ on one helix interact with Leu-8′ and Leu-15′ on the adjacent helix. The helical packing residues are identical in different subunits of M2 segments (except Ile-13′ in γ-subunit), which indicates that the homo-pentameric model is compatible with hetero-pentameric M2 pore assemblies. The external residues are Thr-3′, Ala-4′, Val-7′, Ala-10′, Gln-11′, Phe-14′, Leu-17′, and Thr-18′ (*green*). The external residues place their side chains away from the pore and would interact with other helices in the full-length receptor. The narrowest constriction in the pore occurs at Leu-9′ (αLeu-251), which closes pore with side chain to side chain packing interactions (Fig. 2, *a* and c). Leu-9′ is a key residue in maintaining the closed form of the channel (Revah et al., 1991; Unwin, 1993,1995; Labarca et al., 1995). In general, the pore-lining residues are hydrophobic, which would create an apolar seal and prevent the passage of ions.

Comparison of the AChR M2 channel models

Our model of the M2 segments differs considerably from the M2 structure proposed by Miyazawa et al. based on their low-resolution cryo-EM electron density map (Miyazawa et al., 2003) (PDB code 1OED). The Cα RMSD between the structures is 5.1 Å. As shown in Fig. 2, *b* and *d*, the cryo-EM model displays a smaller tilt with respect to the bilayer (5° vs. 12°). Moreover, the helix-helix packing angle is near 0° (parallel) in the cryo-EM model, which is rarely seen in membrane proteins (Bowie, 1997). A 0° helix packing angle is generally not compatible with close side-chain packing for long helices (Crick, 1953; Chothia et al., 1981). Indeed the cryo-EM model is more loosely packed and has a less tightly closed pore (see below). The orientations of the side chains are quite different in the two structures, as illustrated by the orientation of Leu-9′ (Fig. 2).

Comparison of the M2 channel structure with solid-state NMR data

Solid-state NMR (ssNMR) spectroscopy on oriented lipid bilayer samples can determine the backbone conformation of the peptides (α-helix or β-sheet) and their orientation in the membrane (Ketchem et al., 1993; Opella et al., 1999; Kim et al., 2001; Wang et al., 2001). With ssNMR one can determine the rotational orientation of a helix about its axis and the helical axis tilt angle with respect to the bilayer normal (i.e., magnetic field). The values for these two parameters can be calculated from the ^{15}N chemical shift and ^{1}H-^{15}N dipolar coupling frequencies measured from a 2D PISEMA spectrum. For helical proteins, these spectra exhibit characteristic circular patterns of resonances called PISA (polarity index slant angle) wheels. The helix tilt angle with respect to the bilayer normal is reflected in the size and the location of the PISA wheels (Marassi and Opella, 2000; Wang et al., 2000). The rotation of resonances around the wheel reflects the rotation of the helix around its axis (Opella et al., 1999; Wang et al., 2001). If the helix-helix crossing point and the helix-helix separation distance are also known, a unique structure can be built of the helical bundle. Thus, the PISA wheel can provide powerful constraints for model building, but does not uniquely define a helical bundle structure.

In Fig. 3 we compare the experimentally determined PISEMA spectrum of the AchR M2 δ-subunit peptide (Marassi et al., 1999) with spectra derived from our model and the cryo-EM model. The PISEMA spectrum of an ideal helix should be elliptical. The experimental PISEMA spectrum (Fig. 3 *a*) shows some distortions, however. These deviations arise either from slight variations in the backbone dihedral angles or ^{15}N chemical shift tensors, but there is no sign of a kink in the AchR M2 δ-peptide (Opella et al., 1999). As can be seen in Fig. 3, the size, location, and rotation of the PISA wheel derived from our model more closely matches the experimental spectrum than the wheel from the cryo-EM model. According to Opella and co-workers, the experimental spectrum is consistent with a helix tilt angle of 12° from the lipid bilayer normal, in perfect agreement with our model (12°), but not with the cryo-EM model (5°). The wheel rotation based on our model also shows excellent agreement with the experimental PISA

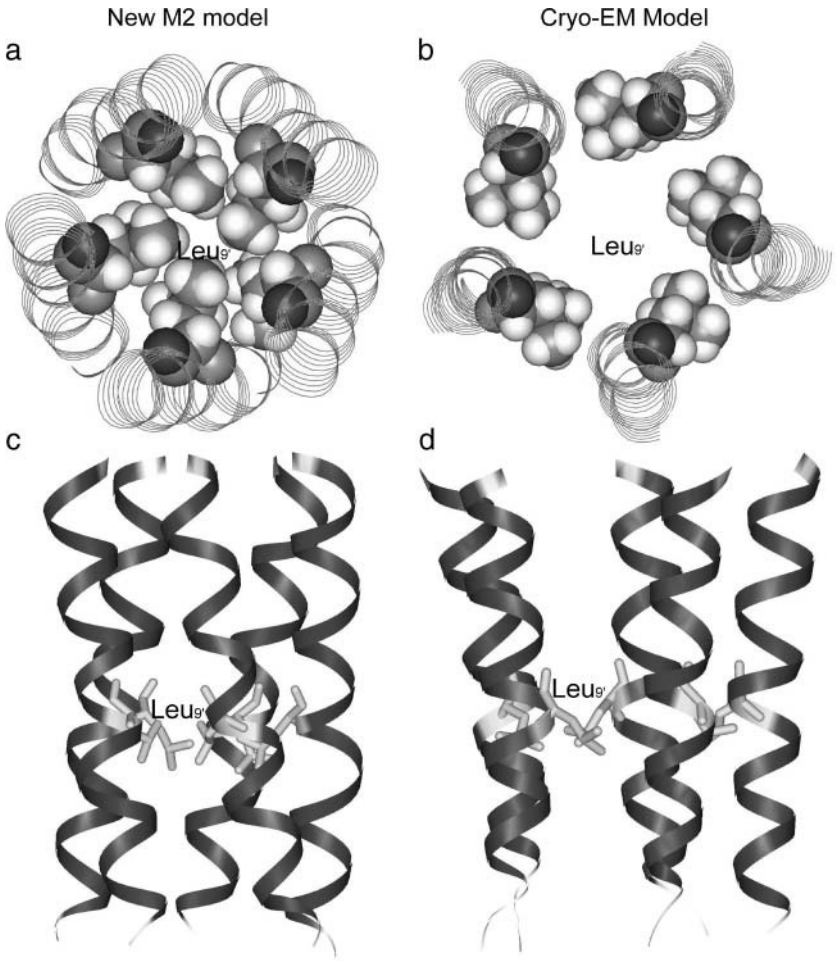

FIGURE 2 Comparison of the models of AChR M2 channel. (*a* and *c*) The closed form of M2 channel from our modeling. A residue critical to the channel function, Leu-9′ (αLeu-251) is the closest residue to the pore axis and is directed inward, helping to seal the ion pore. (*b* and *d*) The M2 segments from the cryo-EM model (PDB code 1OED).

wheel. The pore-lining residues (*shaded*) lie on the upper, left side of the wheel derived from our model and the experimental spectrum. These residues, however, make up the lower, left portion of the cryo-EM wheel, implying that that cryo-EM structure has a helix axis rotation angle different from the ssNMR observations. Even though our model is based solely on helix packing interactions, the helical orientations are perfect agreement with ssNMR data, suggesting that the helical tilt and rotation of M2 peptide is derived from inter-peptide interactions, not from the interaction between the peptides and the lipids.

Comparison with the chemical modification results

Karlin and co-workers determined the reactivity of cysteines substituted in the M2 channel to thiol-modifying reagents (Pascual and Karlin, 1998). This method is referred to as the substituted-cysteine accessibility method (SCAM). The reaction rates were quantified for nine residues in the presence and absence of the Ach, which opens the channel. Because reaction rates can be affected by a number of factors, correlation of SCAM results with structural data is complex. Nevertheless, one would expect that reaction rates should be reasonably correlated with residue accessibility.

For the closed form of the channel, residues αL-245(3′) through αL-258(16′) reacted relatively slowly with MTSEA, but residues αT-244(2′) and αE-262(20′) reacted rapidly. These results are consistent with our model. As shown in Fig. 4, position 2′ and 19′ are the last pore-lining residues and would be accessible to solvent. Residues 5′ through 16′, however, form a tightly packed, hydrophobic seal that would be inaccessible to the water-soluble reagent. In contrast, the pore of the cryo-EM model is relatively open. An MTSEA molecule would not necessarily be excluded and fits within the pore near Leu-9′ or at other pore depths (Fig. 4, *right panel*).

Of the nine residues tested by SCAM, three showed low accessibility in both the closed and open form of the channel {αL-245(3′), αS-248(6′) and αS-252(10′)}. These results suggest that 3′, 6′, and 10′ positions are likely to be pointing away from the channel or involved in helix packing. These residues are circled in Fig. 5, which shows the distances from the Cα atoms to the pore axis. In our model, Thr-3′ and Ala-

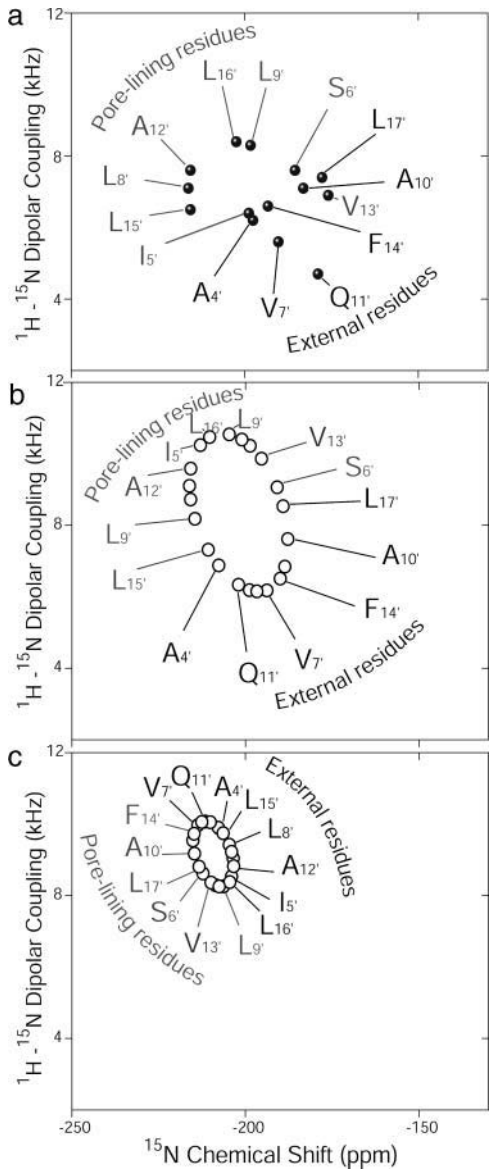

FIGURE 3 Experimental and simulated ssNMR PISEMA spectra of M2. (*a*) The experimentally determined PISEMA spectrum of residue 4′ to 17′ of the M2 peptide in oriented lipid bilayers (Marassi et al., 1999). (*b*) The simulated PISEMA spectrum created from our M2 model. The spectrum shows a match of rotation of the PISA wheel to the experimental spectrum and the helix tilt angle of 12°. (*c*) The simulated PISEMA spectrum created from the cryo-EM model. Residues are presented according to pore lining (*gray*) and external (*black*).

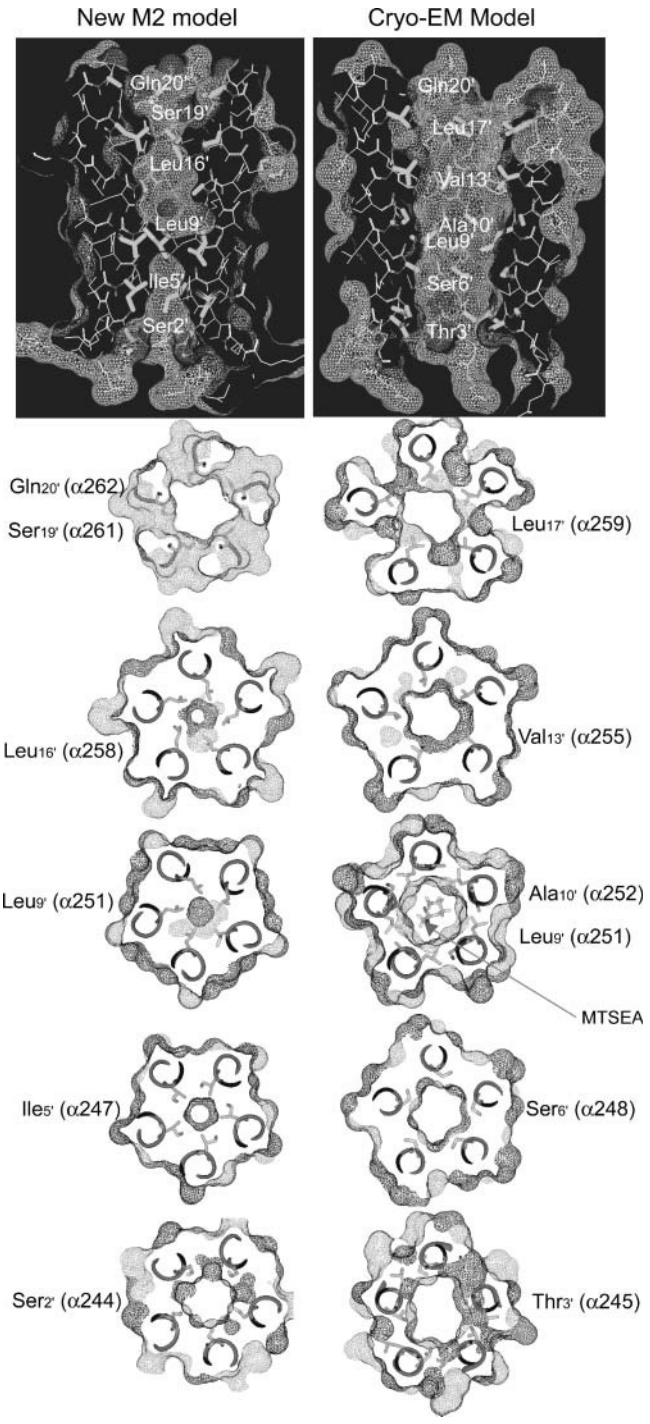

FIGURE 4 M2 channel models viewed perpendicular to the pore axis and in slices along the pore axis. (*Left*) Views of our M2 model. The molecular surface rendering and the slices show the constriction of the pore by the Leu-9′ side chains and other side chains. (*Right*) Views of the cryo-EM model. The size of the pore is almost equivalent from extracellular side (*top*) to the intracellular side (*bottom*). An MTSEA molecule is docked into the pore and shown in the slice with Leu-9′. The surfaces were generated using the program insightII (Accelrys) with probe radius of 1.4 Å.

10′ point externally and Ser-6′ is a helix-packing residue (Fig. 5, *a* and *c*). In contrast, these residues are all pore-lining residues in the cryo-EM model (Fig. 5, *b* and *d*).

The other six residues tested in the SCAM experiments showed significantly increased reactivity upon channel opening and are outlined with diamonds in Fig. 5, *a* and *b*. These residues should be close to the channel lining, assuming a relatively modest structural change opens the pore, which is suggested by cryo-EM electron density maps.

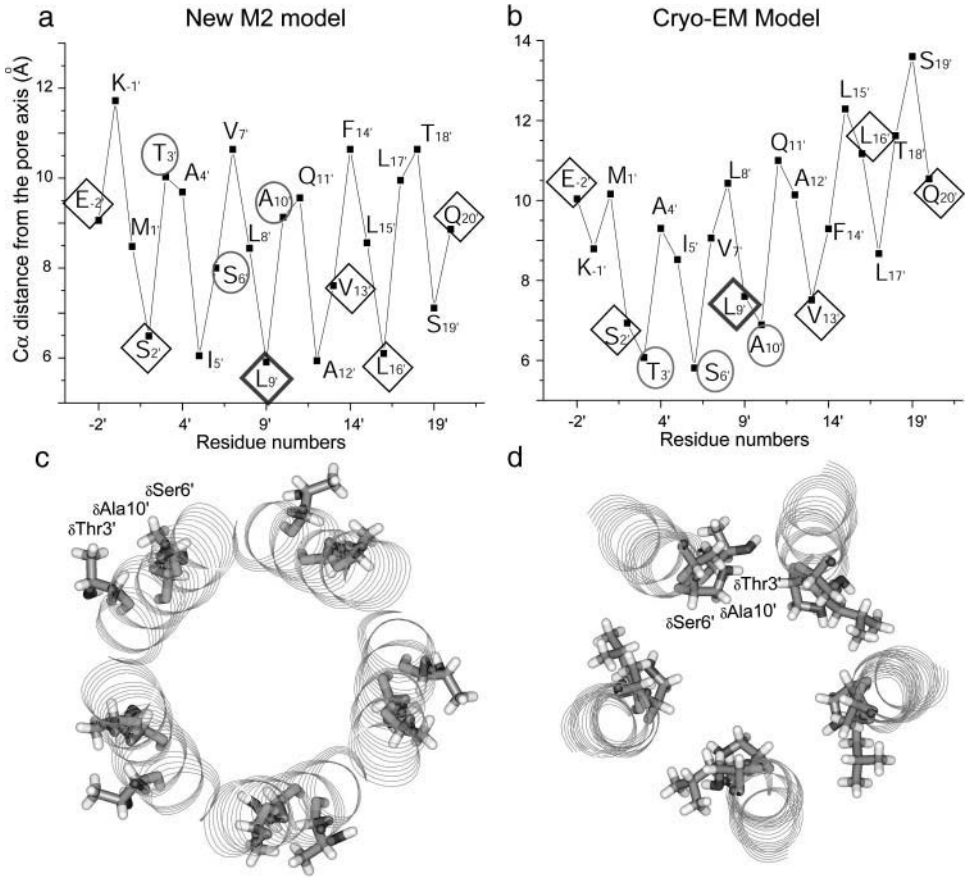

FIGURE 5 Comparison of SCAM results to the structures. (*a*) The Cα-to-pore-axis distances from our model. The pore-lining residues have shorter distances (closer to the axis) and the lipid-facing residues have longer distances. The helix-packing residues have intermediate distances. In the SCAM experiments (Pascual and Karlin, 1998), Thr-3′, Ser-6′, and Ala-10′ (*circles*) showed low accessibility in both closed and open forms of channel and would be expected to be exterior residues (large distances). Potential channel-lining residues are marked with diamonds. The key position, Leu-9′, is shaded. (*b*) The Cα-to-pore-axis distances from the cryo-EM model; the three residues inaccessible to SCAM reagents in both the closed and the open forms, Thr-3′, Ser-6′, and Ala-10′ (*circles*) have small Cα-to-pore-axis distances and line the channel. (*c* and *d*) A comparison of our model (*c*) and the cryo-EM model (*d*) viewed down the pore axis showing the location and accessibility of Thr-3′, Ser-6′, and Ala-10′, which are oriented away from the pore axis in our model in accord with the SCAM data.

Both models are reasonably consistent with this SCAM data, except that Leu-16′ is external in the cryo-EM model. Thus, our model appears to be more consistent with the SCAM results than the cryo-EM model.

The role of αLeu-251

αL-251(9′) is the most conserved residue in the M2 helix (Unwin, 1993) and has been identified as a key residue in the function of the pore (Revah et al., 1991; Labarca et al., 1995). Mutations at Leu-9′ increase the opening sensitivity of the channel (Revah et al., 1991; Labarca et al., 1995). Photolabeling experiments by Blanton et al. (1998) also indicate that Leu-9′ is located in the pore lining. Their hydrophobic photolabel efficiently reacted with the residues of the pore, specifically the Leu-9′ position. They suggest that Leu-9′ is involved in a key symmetric hydrophobic interaction that closes the gate. Our model is consistent with this hypothesis.

Although we did not impose any structural restraints on the Leu-9′ position, the narrowest part of the pore occurs at Leu-9′ in our model (Figs. 2 *a* and 4, *left panel*). Leu-9′ has the shortest Cα-to-pore-axis distance of any residue (Fig. 5 *a*) and makes tight, side chain to side chain packing interactions. In the cryo-EM structure, however, Ser-6′ is the closest residue to the pore axis and Leu-9′ is the fifth closest residue. The position and tight packing of Leu-9′ in our model explains why this residue is conserved and why mutations of Leu-9′ would destabilize the closed form of the channel and thereby enhance channel opening.

The channel gate

The position of the gate in the AchR channel has been controversial. αL-251(9′) has been suggested as the channel gate based on its strong sequence conservation and its sensitivity to mutations. This position is also been proposed to form a constriction, or gate, based on cryo-EM images. SCAM results from Karlin and co-workers suggested that the gate is more intracellular, however, and near residue αT-244(2′). Their results indicate that position 2′ is accessible from the extracellular side of the membrane in the closed state. In our model, we would expect that ions could not pass beyond residue 16′ from the extracellular side or residue 5′ from the intracellular side. We propose that the gate is comprised of a multilayer hydrophobic seal involving the close packing of residues 5′, 9′, 12′, and 16′.

Ion selectivity

Our model contains a ring of negatively charged residues at position −2′ and 20′, which is at the both intracellular and

extracellular mouth of the pore. Specifically, the side chain of position $-2'$ is pointing toward the pore on the intracellular side. Position $20'$ on the extracellular side, although not pointing directly into the pore, also contains negatively charged side chains, which would be expected to limit the anion flow. These anionic rings were proposed to impart cation selectivity based on early electrophysiology experiments, and mutations at both these positions affected the rate of cation transport (Imoto et al., 1986,1988). In the heteropentameric AChR channel (α, α, β, γ, and δ subunits), position $-2'$ contains four Glu and one Gln. At the extracellular side of the pore, position $20'$, contains two Glu, one Asp, and two Gln residues (Fig. 1 *a*). Thus, our model suggests the mouth of the pore of both intracellular and extracellular sides are electrically negative charged and could act as the energy barrier for anion entry into the pore (Kienker et al., 1994).

Our model is also consistent with results indicating that position $2'$ (αT-244) plays a role in cation selectivity. In particular, mutations at position $2'$ are known to affect the conductance of different monovalent cations (Imoto et al., 1991; Villarroel et al., 1991). Changes in side-chain volume affected the conductance of the larger cations (Rb^+ and Cs^+) more than that of Na^+. In our model, the pore is wider at position $2'$ than near Ile-$5'$, Leu-$9'$ and Leu-$16'$ (Fig. 4, *left panel*). An increase in side-chain volume at position $2'$ would be expected to constrict the pore and interfere with the conductance of the larger ions.

CONCLUSION

Our model is based on a peptide and it is possible that the peptide structure differs from the channel in the full-length protein. Thus, the differences between the cryo-EM model and ours may reflect genuine structural differences between the peptide and the full-length protein. Alternatively, the protein may adopt partially open form in the crystals, which would be consistent with the relatively open channel in the cryo-EM model. The results obtained from ssNMR results on the peptide, as well as mutagenesis, electrophysiology and chemical modification experiments on the full-length protein all seem consistent with our model, however. Moreover, we have shown that our method can correctly model the structure of peptides extracted from full-length proteins (Kim et al., 2004). As we did not use any of the experimental data in building the model, they provide independent validation of the model. Thus, we believe our model is likely to represent the structure of the closed form of the channel and should therefore be useful in designing and interpreting future studies on the AChR structure and function.

We thank Salem Faham, Sehat Nauli, Sarah Yohannan, Chongwoo Kim, and Nathan Cho for helpful comments on the manuscript.

This work was supported by National Institutes of Health grant RO1 GM063919.

REFERENCES

Akabas, M. H., and A. Karlin. 1995. Identification of acetylcholine receptor channel-lining residues in the M1 segment of the alpha-subunit. *Biochemistry*. 34:12496–12500.

Blanton, M. P., L. J. Dangott, S. K. Raja, A. K. Lala, and J. B. Cohen. 1998. Probing the structure of the nicotinic acetylcholine receptor ion channel with the uncharged photoactivatable compound [^{3}H]diazofluorene. *J. Biol. Chem.* 273:8659–8668.

Bower, M. J., F. E. Cohen, and R. L. Dunbrack. 1997. Prediction of protein side-chain rotamers from a backbone-dependent rotamer library: A new homology modeling tool. *J. Mol. Biol.* 267:1268–1282.

Bowie, J. U. 1997. Helix packing in membrane proteins. *J. Mol. Biol.* 272:780–789.

Brunger, A. T., P. D. Adams, G. M. Clore, W. L. Delano, P. Gros, R. W. Grosse-Kunstleve, J.-S. Jiang, J. Kuszewski, M. Nilges, N. S. Pannu, R. J. Read, L. M. Rice, T. Simonson, G. L. Warren. 1998. Crystallography and NMR system. *Acta Cryst.* D54:905–921.

Chekmenev, E. Y., Q. Zhang, K. W. Waddell, M. S. Mashuta, and R. J. Wittebort. 2004. 15N chemical shielding in Glycyl Tripeptdies: Measurement by solid-state NMR and correlation with x-ray structure. *J. Am. Chem. Soc.* 126:379–384.

Chothia, C., M. Levitt, and D. Richardson. 1981. Helix to helix packing in proteins. *J. Mol. Biol.* 145:215–250.

Corringer, J.-P., N. Le Novère, and J.-P. Changeux. 2000. Nicotinic receptors at the amino acid level. *Annu. Rev. Pharmacol. Toxicol.* 40:431–458.

Crick, F. 1953. The packing of α-helices: simple coiled coils. *Acta Crystallogr.* 6:689–697.

Hucho, F., W. Oberthur, and F. Lottspeich. 1986. The ion channel of the nicotinic acetylcholine receptor is formed by the homologous helices M II of the receptor subunits. *FEBS Lett.* 205:137–142.

Imoto, K., C. Busch, B. Sakmann, M. Mishina, T. Konno, J. Nakai, H. Bujo, Y. Mori, K. Fukuda, and S. Numa. 1988. Rings of negatively charged amino acids determine the acetylcholine receptor channel conductance. *Nature*. 335:645–648.

Imoto, K., T. Konno, J. Nakai, F. Wang, M. Mishina, and S. Numa. 1991. A ring of uncharged polar amino acids as a component of channel constriction in the nicotinic acetylcholine receptor. *FEBS Lett.* 289: 193–200.

Imoto, K., C. Methfessel, B. Sakmann, M. Mishina, Y. Mori, T. Konno, K. Fukuda, M. Kurasaki, H. Bujo, Y. Fujita, and S. Numa. 1986. Location of a delta-subunit region determining ion transport through the acetylcholine receptor channel. *Nature*. 324:670–674.

Karlin, A. 2002. Emerging structure of the nicotinic acetylcholine receptors. *Nat. Rev. Neurosci.* 3:102–114.

Kelley, L. A., S. P. Gardner, and M. J. Sutcliffe. 1996. An automated approach for clustering an ensemble of NMR-derived protein structures into conformationally-related subfamilies. *Protein Eng.* 9:1063–1065.

Ketchem, R. R., W. Hu, and T. A. Cross. 1993. High-resolution conformation of gramicidin A in a lipid bilayer by solid-state NMR. *Science*. 261:1457–1460.

Kim, S., and T. A. Cross. 2002. Uniformity, ideality and hydrogen bonds in transmembrane α helices. *Biophys. J.* 83:2084–2095.

Kim, S., A. K. Chamberlain, and J. U. Bowie. 2003. A simple method for modeling transmembrane helix oligomers. *J. Mol. Biol.* 329:831–840.

Kim, S., A. K. Chamberlain, and J. U. Bowie. 2004. Membrane channel structure of *Helicobacter pylori* vacuolating toxin: Role of multiple GxxxG motifs in cylindrical channels. *Proc. Natl. Acad. Sci. USA*. 101:5988–5991.

Kim, S., J. R. Quine, and T. A. Cross. 2001. Complete cross-validation and R-factor calculation of a solid-state NMR derived structure. *J. Am. Chem. Soc.* 123:7292–7298.

Kienker, P., G. Tomaselli, M. Jurman, and G. Yellen. 1994. Conductance mutations of the Nicotinic Acetylcholine Receptor do not act by a simple electrostatic mechanism. *Biophys. J.* 66:325–334.

Labarca, C., M. W. Nowak, H. Zhang, L. Tang, P. Deshpande, and H. A. Lester. 1995. Channel gating governed symmetrically by conserved leucine residues in the M2 domain of nicotinic receptors. *Nature.* 376:514–516.

Leonard, R. J., C. Labarca, P. Charnet, N. Davidson, and H. A. Lester. 1988. Evidence that the M2 membrane-spanning region lines the ion channel pore of the nicotinic receptor. *Science.* 242:1578–1581.

Lester, H. A. 1992. The permeation pathway of neurotransmitter-gated ion channels. *Annu. Rev. Biophys. Biomol. Struct.* 21:267–292.

Marassi, F. M., and S. J. Opella. 2000. A solid-state NMR index of helical protein structure and topology. *J. Magn. Reson.* 144:150–155.

Marassi, F. M., J. J. Gesell, A. P. Valente, Y. Kim, M. Oblatt-Montal, M. Montal, and S. J. Opella. 1999. Dilute spin-exchange assignment of solid-state NMR spectra of oriented proteins: acetylcholine M2 in bilayers. *J. Biomol. NMR.* 14:141–148.

Miyazawa, A., Y. Fujiyoshi, and N. Unwin. 2003. Structure and gating mechanism of the acetylcholine receptor pore. *Nature.* 423:949–955.

Oiki, S., W. Danho, V. Madison, and M. Montal. 1988. M2 delta, a candidate for the structure lining the ionic channel of the nicotinic cholinergic receptor. *Proc. Natl. Acad. Sci. USA.* 85:8703–8707.

Opella, S. J., F. M. Marassi, J. J. Gesell, A. P. Valente, Y. Kim, M. Oblatt-Montal, and M. Montal. 1999. Structures of the M2 channel-lining segments from nicotinic acetylcholine and NMDA receptors by NMR spectroscopy. *Nat. Struct. Biol.* 6:374–379.

Pascual, J. M., and A. Karlin. 1998. State-dependent accessibility and electrostatic potential in the channel of the acetylcholine receptor: inferences from rates of reaction of thiosulfonates with substituted cysteines in the M2 segment of the alpha subunit. *J. Gen. Physiol.* 111:717–739.

Patrick, J., and J. Lindstrom. 1973. Autoimmune response to acetylcholine receptor. *Science.* 180:871–872.

Ramamoorthy, A., C. H. Wu, and S. J. Opella. 1995. Three-dimensional solid-state NMR experiment that correlates the chemical shift and dipolar coupling frequencies of two heteronuclei. *J. Magn. Reson. B.* 107:88–90.

Revah, F., D. Bertrand, J. L. Galzi, A. Devillers-Thiery, C. Mulle, N. Hussy, S. Bertrand, M. Ballivet, and J. P. Changeux. 1991. Mutations in the channel domain alter desensitization of a neuronal nicotinic receptor. *Nature.* 353:846–849.

Smith, L. J., K. A. Bolin, H. Schwalbe, M. W. MacArthur, J. M. Thornton, and C. M. Dobson. 1996. Analysis of main chain torsion angles in proteins: prediction of NMR coupling constants for native and random coil conformations. *J. Mol. Biol.* 255:494–506.

Unwin, N. 1993. Nicotinic acetylcholine receptor at 9 Å resolution. *J. Mol. Biol.* 229:1101–1124.

Unwin, N. 1995. Acetylcholine receptor channel imaged in the open state. *Nature.* 373:37–43.

Villarroel, A., S. Herlitze, M. Koenen, and B. Sakmann. 1991. Location of a threonine residue in the alpha-subunit M2 transmembrane segment that determines the ion flow through the acetylcholine receptor channel. *Proc. R. Soc. Lond. B Biol. Sci.* 243:69–74.

Vincent, A., J. McConville, M. E. Farrugia, M. E. Farrugia, J. Bowen, P. Plested, T. Tang, A. Evoli, I. Matthews, G. Sims, P. Dalton, L. Jacobson, A. Polizzi, F. Blaes, B. Lang, D. Beeson, N. Willcox, J. Newsom-Davis, and W. Hoch. 2003. Antibodies in myasthenia gravis and related disorders. *Ann. N. Y. Acad. Sci.* 998:324–335.

Wang, J., J. Denny, C. Tian, S. Kim, Y. Mo, F. Kovacs, Z. Song, K. Nishimura, Z. Gan, R. Fu, J. R. Quine, and T. A. Cross. 2000. Imaging membrane protein helical wheels. *J. Magn. Reson.* 144:162–167.

Wang, J., S. Kim, F. Kovacs, and T. A. Cross. 2001. Structure of the transmembrane region of the M2 protein H^+ channel. *Protein Sci.* 10:2241–2250.

White, B. H., and J. B. Cohen. 1992. Agonist-induced changes in the structure of the acetylcholine receptor M2 regions revealed by photoincorporation of an uncharged nicotinic noncompetitive antagonist. *J. Biol. Chem.* 267:15770–15783.

Wu, C. H., A. Ramamoorthy, and S. J. Opella. 1994. High-resolution heteronuclear dipolar solid-state NMR spectroscopy. *J. Magn. Reson. A.* 109:270–274.

Zhang, H., and A. Karlin. 1997. Identification of acetylcholine receptor channel-lining residues in the M1 segment of the beta-subunit. *Biochemistry.* 36:15856–15864.